frontiers | Frontiers in Ecology and Evolution

TYPE Original Research
PUBLISHED 03 November 2023
DOI 10.3389/fevo.2023.1238334

OPEN ACCESS

EDITED BY
Alessio Fabbrini,
University College London,
United Kingdom

REVIEWED BY
Thomas Mark Cronin,
United States Geological Survey
(USGS), United States
Selvaraj Kandasamy,
Central University of Kerala, India
Janne Repschlaeger,
Max Planck Institute for Chemistry,
Germany

*CORRESPONDENCE
Jaime Y. Suárez-Ibarra
jysuarezibarra@gmail.com;
suarezij@natur.cuni.cz

†PRESENT ADDRESS
Tiago M. Freire,
Institut für Geologie & Mineralogie,
Universität zu Köln, Köln, Germany

RECEIVED 11 June 2023
ACCEPTED 12 October 2023
PUBLISHED 03 November 2023

CITATION
Suárez-Ibarra JY, Freire TM, Frozza CF, Pinho TML, Petró SM, Dias BB, Chalk TB, Chaabane S, Srivastava M, Costa KB, Toledo FAL, de Garidel-Thoron T, Coimbra JC and Pivel MAG (2023) Surface fertilisation and organic matter delivery enhanced carbonate dissolution in the western South Atlantic.
Front. Ecol. Evol. 11:1238334.
doi: 10.3389/fevo.2023.1238334

Surface fertilisation and organic matter delivery enhanced carbonate dissolution in the western South Atlantic

Jaime Y. Suárez-Ibarra[1*], Tiago M. Freire[2†], Cristiane F. Frozza[2], Tainã M. L. Pinho[3], Sandro M. Petró[4], Bruna B. Dias[5,6], Thomas B. Chalk[7], Sonia Chaabane[7,8,9], Medhavi Srivastava[1], Karen B. Costa[10], Felipe A. L. Toledo[10], Thibault de Garidel-Thoron[7], João C. Coimbra[11] and María A. G. Pivel[11]

[1]Ústav Geologie a Paleontologie, Přírodovědecká fakulta, Univerzita Karlova, Praha, Czechia, [2]Programa de Pós-Graduação em Geociências, Instituto de Geociências, Universidade Federal do Rio Grande do Sul, Porto Alegre, Brazil, [3]Alfred Wegener Institute, Helmholtz Center for Polar and Marine Research, Bremerhaven, Germany, [4]itt OCEANEON – Instituto Tecnológico de Paleoceanografia e Mudanças Climáticas, Universidade do Vale do Rio dos Sinos, São Leopoldo, RS, Brazil, [5]School of Arts, Science and Humanities, University of São Paulo, Cidade Universitária, São Paulo, Brazil, [6]Murray Edwards College, University of Cambridge, Cambridge, United Kingdom, [7]Aix-Marseille Université, CNRS, IRD, INRAE, CEREGE, Europôle Méditerranéen de l'Arbois, Aix-en-Provence Cedex, France, [8]Department of Climate Geochemistry, Max Planck Institute for Chemistry, Mainz, Germany, [9]Fondation pour la recherche sur la biodiversité (FRB-CESAB), Montpellier, France, [10]Laboratório de Paleoceanografia do Atlântico Sul, Instituto Oceanográfico, Universidade de São Paulo, Praça do Oceanográfico, São Paulo, Brazil, [11]Centro de Estudos de Geologia Costeira e Oceânica (CECO), Instituto de Geociências, Universidade Federal do Rio Grande do Sul, Porto Alegre, Brazil

The last glacial inception was characterised by rapid changes in temperature, atmospheric pCO_2, and changes in the water mass geometry of the major ocean basins. Although several climatic feedback mechanisms have been proposed to explain the glacial/interglacial cycles witnessed in the Quaternary, the exact mechanistic responses of these processes are still under constrained. In this study we use proxies including planktonic foraminifera compositional assemblages and oxygen stable isotopes to reconstruct past changes in sea surface productivity, stratification, and carbonate dissolution. We use core SIS-249 (2,091 mbsl, western South Atlantic 30°S 47°W), spanning 30–110 thousand years ago (ka), and currently bathed by modern Northern Component Water. We test existing hypotheses suggesting that the orbital obliquity cycle modulates the biological pump in the study area. Spectral analysis run on our synthesised productivity proxies recognises a ~43 kyr-cycle, related to the obliquity cycle. We propose that the enhanced productivity is produced by two mechanisms: i) the glacial upwelling of subsurface nutrient-rich waters and, ii) the continental (wind-driven dust and riverine outflows) fertilisation of the photic zone, with the latter process being obliquity-paced. We also suggest that not only the increased organic matter export but also a change in its bioavailability (from refractory to labile) led to calcium carbonate dissolution, as the degradation of the more soluble organic matter decreased the pH of the glacial bottom water, partially dissolving the calcium carbonate. Although our correlation analyses show a strong benthic-pelagic coupling through the relation between the

enhanced biological pump and carbonate dissolution (p<0.05, r=0.80), we cannot reject the potential of corrosive Southern Component Water bathing the site during the glacial. Finally, we highlight that these processes are not mutually exclusive and that both can be modulated by the obliquity cycle.

KEYWORDS

planktonic foraminifera, primary productivity, stratification, southern Brazilian continental margin, late Quaternary

1 Introduction

Glacial-interglacial cycles are characterised by cold stages, witnessing decreased temperatures and carbon dioxide (CO_2) concentrations, the growth of ice sheets and the rearrangement of water mass geometry (Lisiecki and Raymo, 2005; Ahn and Brook, 2008; Doughty et al., 2021; Shackleton et al., 2021; Menking et al., 2022). During these cycles, multiple mechanisms contribute to CO_2 drawdown, resulting in a reduction of atmospheric CO_2 levels. These mechanisms include changes in ocean carbonate chemistry (Rickaby et al., 2010), boosted biological pump (Martin, 1990; Sigman and Boyle, 2000), enhanced calcium carbonate preservation (Archer and Maier-Reimer, 1994; Brovkin et al., 2012; Doss and Marchitto, 2013) and expanded Antarctic sea ice (Stephens and Keeling, 2000; Sigman et al., 2010), among others.

The growth of southern ice sheets during glacial stages resulted in a reorganised Atlantic Ocean, marked by the expansion of corrosive carbon-rich deep-water masses to shallower depths (e.g., Duplessy et al., 1988; Curry and Oppo, 2005; Govin et al., 2009; Howe et al., 2016a; Howe et al., 2018) and, the redistribution of nutrients, boosting the biological pump and enhancing the oceans' capacity to sequestrate atmospheric CO_2 during glacial periods (Broecker, 1982; Sigman and Boyle, 2000; Skinner, 2009; Rickaby et al., 2010; Ziegler et al., 2013). Yet, the precise way in which these two mechanisms act and interact is still under debate.

For the western South Atlantic, several studies have documented the impact of glacial-interglacial stages on the carbon cycle (Gu et al., 2017; Pereira et al., 2018; Portilho-Ramos et al., 2019; Frozza et al., 2020; Suárez-Ibarra et al., 2022) and past bottom water mass geometry (Howe et al., 2016a; Howe et al., 2016b; Howe et al., 2018). One important characteristic of these climatic variations is the effect on calcium carbonate preservation, as it plays an important role in the global carbon cycle. The reorganised "glacial" Atlantic Ocean affects the calcium carbonate preservation both hemispheres negatively (i.e., Chalk et al., 2019; Petró et al., 2021). In addition, another well-known mechanism affected by the glacial-interglacial cycles intemperate zones is the expansion of the southwesterly winds (Toggweiler et al., 2006), displacing the north limit of the wind belt (from 40°S to 30°S latitude, Gili et al., 2017). The change in the wind belt position, associated with an increasing wind strength paced by the obliquity cycle, has been pointed to enhance the terrestrial nutrient supply (Lopes et al., 2021). This enhancement is thought to increase the productivity of the marine ecosystems.

Another critical factor that can influence calcium carbonate preservation is the biological pump, transporting organic carbon from the surface to the deep ocean. In the western South Atlantic, Suárez-Ibarra et al. (2022) documented that high primary productivity during the last glacial exported a higher amount of organic matter to the seafloor, where it is remineralised. This process releases $CO_{2(aq)}$, which increases acidity, affecting the preservation of calcium carbonate, and raising questions about the potential of an enhanced glacial biological pump to efficiently sequester carbon in the sediments.

Yet, the extent of the mechanisms driving calcium carbonate preservation and carbon cycling in the western South Atlantic remains to be fully elucidated. It is required an integrated approach encompassing both benthic and pelagic systems to provide insights into the underlying dynamics during the last interglacial-glacial interval. Thus, we use planktonic and benthic foraminifera counts, geochemical analysis (oxygen stable isotopes, $\delta^{18}O$), sedimentological quantifications (size fraction) and various statistical tools such as correlation, spectral and clustering analyses from the western South Atlantic. By comparing our data with other records from the southern and southeastern Brazilian continental margin, our objectives are: i) to infer the mechanisms that modulate the oceanic fertilisation, ii) to quantify the potential effect of sea surface productivity on carbonate dissolution, and iii) to test the influence of the orbital obliquity cycle on surface and bottom conditions.

2 Oceanographic setting

The modern upper ocean circulation of the subtropical South Atlantic is governed by the subtropical gyre (Peterson and Stramma, 1991). The western boundary of the subtropical gyre is impacted mainly by the Brazil Current, which transports warm, salty, oligotrophic waters at the surface (tropical surface water, temperature > 20°C; salinity > 36 psu; Peterson and Stramma, 1991; Stramma and England, 1999). Below this tropical surface water (~100 m) flow the cooler and more nutrient-rich South Atlantic Central Water (Stramma and England, 1999), and the Antarctic Intermediate Water with lower salinity and temperature and higher

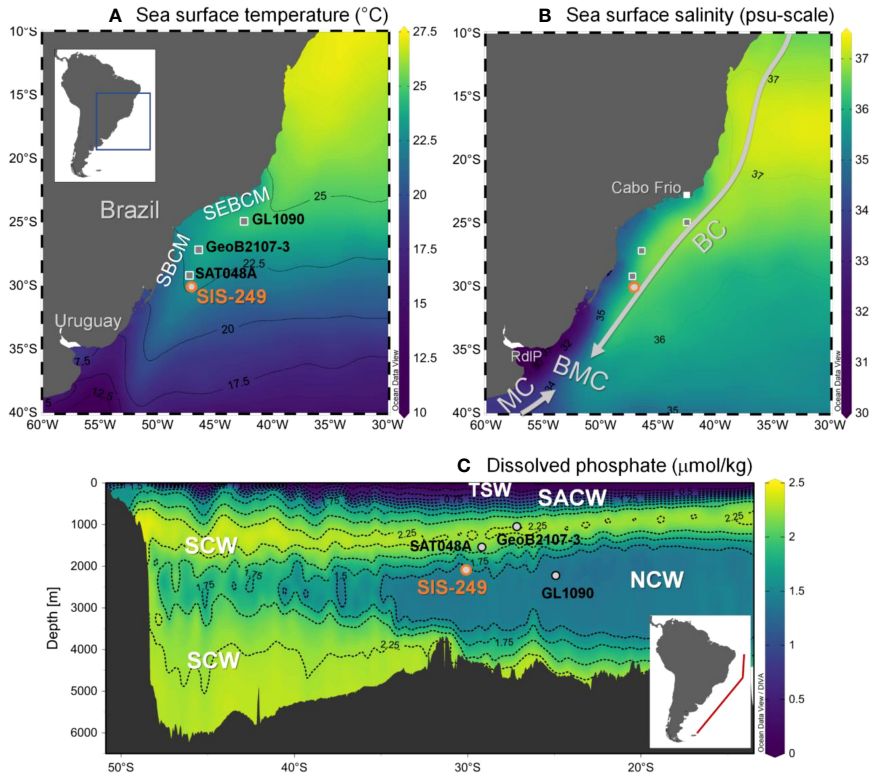

FIGURE 1
(A) Annual mean sea surface temperature and **(B)** annual mean sea surface salinity from the World Ocean Atlas 2013 (WOA13, Locarnini et al., 2013) relative to core SIS-249 location (in orange). Other cores analysed in this study are indicated in grey (GeoB2107-3, Gu et al., 2017; GL1090, Santos et al., 2017a; SAT048A, Suárez-Ibarra et al., 2022). **(C)** Vertical dissolved phosphate section profile through the western South Atlantic according to the World Ocean Circulation Experiment (WOCE, Section A17; Schlitzer, 2000) and recovery depth of cores. SBCM, Southern Brazilian Continental Margin; SEBCM, Southeastern Brazilian Continental Margin; RdlP, Río de la Plata; MC, Malvinas Current; BC, Brazil Current; BMC , Brazil-Malvinas Confluence; TSW, Tropical Surface Water; SACW, South Atlantic Central Water; SCW, Southern Component Water; NCW, Northern Component Water. Plotted using Ocean Data View (Schlitzer, 2020).

oxygen values (Stramma and England, 1999). To the South of our study site (Figure 1), at about 38°S, the Brazil Current encounters the cool, fresher, and nutrient-rich waters of the Malvinas Current (temperature < 15°C; salinity < 34.2 psu), forming the Brazil-Malvinas Confluence (Gordon and Greengrove, 1986; Gordon, 1989; Piola et al., 2000). Currently, the seafloor core location is bathed by the southward movement of North Atlantic Deep Water, (hereafter termed generally as Northern Component water, NCW) a water mass that promotes calcium carbonate preservation due to its oversaturation in carbonate ion (CO_3^{2-}). Conversely, Southern Component water (SCW, comprising the Antarctic Intermediate Water, Circumpolar Deep Water and Antarctic Bottom Water), which is undersaturated in CO_3^{2-}, flows northward above and below the NCW at this location, and its increased corrosiveness leads to calcium carbonate dissolution (Broecker and Peng, 1982; Frenz et al., 2003; Frenz and Henrich, 2007).

Close to the coring site (35° S), the Río de la Plata (RdlP), the second largest continental water outflow in South America, reaches the South Atlantic (Matano et al., 2014). The RdlP drains cool and low salinity waters into the coastal region and increases the nutrient availability, enhancing biological productivity along the continental shelves of Uruguay and southern Brazil during austral winter. Northward displacement of the RdlP outflow occurs in response to the variability of the alongshore wind stress (e.g., Braga et al., 2008; Möller et al., 2008). The RdlP outflows can reach 28° S along the modern inner and mid-shelves (Piola et al., 2000; Piola et al., 2005; Möller et al., 2008). In contrast, during austral summer, NE winds restrict the RdlP outflows to the south (~32° S), inhibiting fertilisation by reducing nutrient supply from continental outflows.

3 Materials and methods

3.1 Marine sediment core

The sediment samples used in this study come from the piston core SIS-249, which measures 1.94 metres in length. This core was retrieved from the lower continental slope of the southern Brazilian continental margin at 2,091 metres below sea level (30°05′ S; 47°05′ W, Figure 1). Core SIS-249 was obtained during an oceanographic campaign in the austral spring-summer of 2007 by *Fugro Brasil Ltda* for the Brazilian National Agency of Petroleum, Natural Gas and Biofuels. Due to the presence of shallower allochthonous sands in the uppermost 48 cm of the core, this study focuses on the carbonate-rich pelagic mud and sandy mud, which lie between 48 and 194 cm. Within this interval, we collected 45 samples with a

sampling spacing of 2 to 4 cm to analyse the planktonic foraminifera fossil assemblages and stable isotopes.

3.2 Planktonic foraminifera compositional assemblage

To assess planktonic foraminifera assemblages, each sample (~9 cc) was sequentially weighed, washed over a 63 μm sieve, dried at 55°C, and weighed again. To avoid juvenile specimens, which would induce taxonomic biases, planktonic foraminifera were only picked from the >150 μm size fraction (CLIMAP Project Members, 1976; Peeters et al., 1999). The processed samples were then divided with a micro splitter to recover at least 300 non-fragmented planktonic foraminifera tests per sample, as to support significant statistical variations of around 10% for assemblage analyses (Patterson and Fishbein, 1989). The taxonomic classification on the species level followed Schiebel and Hemleben (2017).

3.3 Age model improvement

The chronology of core SIS-249 was first published by Rodrigues et al. (2018) based on one single Accelerator Mass Spectrometry (AMS) radiocarbon age combined with benthic oxygen stable isotope ($\delta^{18}O$) stratigraphy. The AMS radiocarbon date from Rodrigues et al. (2018) was measured on tests of *Globigerinoides ruber* at 58 cm core-depth and the age model developed in the software AnalySeries 1.1 (Paillard et al., 1996).

In the present study, we improved the age model by using six $\delta^{18}O$ tie-points (two points from the new $\delta^{18}O_{G.rub}$ record and four from $\delta^{18}O_{Uvig}$), which are now correlated with the records from core GL-1090 (Santos et al., 2017a), a nearby core with high-resolution and well-calibrated age model (based on 14 AMS ^{14}C and 13 stable oxygen isotope correlation points to two reference curves: Lisiecki and Raymo, 2005 and Govin et al., 2014). The new refined age model was created in the R-package "Bacon" v. 2.5.3, which implements Bayesian statistics (Blaauw and Christeny, 2011). We considered a propagated error of 2.5 kyr, conservatively estimated based on the mean accumulation rates of cores SIS-249 and GL-1090 (ca. 1.87 and 0.29 cm/kyr, respectively) and the <2 kyr age error from the GL-1090 reference curve (Santos et al., 2017a). The raw AMS radiocarbon age date from Rodrigues et al. (2018) was calibrated within the R-package "bacon", using the Marine20 curve (Heaton et al., 2020) and applying a regional reservoir effect (ΔR) of −85 ± 40 years (Tables S1 and S2). This estimate follows the Marine Reservoir Correction Database (http://calib.org/marine/), considering the ages of Nadal De Masi (1999), Angulo et al. (2005), and Alves et al. (2015).

3.4 Productivity proxies

We reconstruct past sea surface productivity using the ratio between the species *Globigerina bulloides* and *Globigerinoides ruber* (*G.bull/G.rub*), the relative abundance (%) of *Globigerinita glutinata*, and the benthic foraminifera accumulation rate (BFAR).

The *G.bull/G.rub* ratio is used to reconstruct upwelling events (Conan et al., 2002; Toledo et al., 2008) based on the contrasting ecological preferences of both species. The opportunistic species *G. bulloides* is associated with eutrophic waters in upwelling zones (Sautter and Thunell, 1991; Peeters et al., 2002; Zaric et al., 2005; Mohtadi et al., 2007; Lessa et al., 2014), while *G. ruber*, a symbiont-bearing shallow water-dwelling species, is abundant in tropical/subtropical planktonic foraminiferal provinces (Bé and Hutson, 1977; Kučera, 2007; Schiebel and Hemleben, 2017). Moreover, the *G. glutinata* abundance is typically higher in phytoplankton-rich waters and is used as a proxy for paleoproductivity (Conan and Brummer, 2000; Souto et al., 2011; Pereira et al., 2018).

We also applied the BFAR index, calculated here as the total number of benthic foraminifera multiplied by the sediment accumulation rate as it has been shown to be a reliable proxy for the organic carbon flux to the seafloor in the Brazilian margin (Dias et al., 2021). The BFAR index represents the increments of primary productivity export to the seafloor, in which the increases on benthic biomass are associated to the increasing food availability to the benthic community (Herguera and Berger, 1991; Guichard et al., 1997; Jorissen et al., 2007). Thus, these planktonic and benthic foraminiferal proxies together can indicate changes in the fertilisation mechanisms affecting the photic zone (i.e., biological pump, terrestrial nutrient input) and posterior organic matter export.

3.5 Upper water column stratification proxies

To assess changes in sea surface stratification, we studied both the stable isotopic composition of selected planktonic foraminifera species and assemblage counts. As planktonic foraminifera calcitic tests record a mean value corresponding to that of the local water mass properties (i.e., temperature, salinity) at the different depths where they live, their $\delta^{18}O$ signal allows the reconstruction of the seawater conditions at different depth layers (Emiliani, 1954; Ravelo and Hillaire-Marcel, 2007). The species *G. ruber* dwells at surface-shallow depths, while the species *Globorotalia inflata* is a subsurface-thermocline dweller (Chiessi et al., 2007; Groeneveld and Chiessi, 2011; Schiebel and Hemleben, 2017; Lessa et al., 2020). Therefore, the gradient between the $\delta^{18}O$ values of these two species ($\Delta\delta^{18}O_{G.inf\text{-}G.rub}$) indicates a decreased (increased) upper water column stratification according to the lower (higher) $\Delta\delta^{18}O_{G.inf\text{-}G.rub}$ values (Santos et al., 2017b and references therein).

Around 10 specimens of *G. ruber* and *G. inflata* were collected per sample for the $\delta^{18}O$ analyses from the size fraction >250 μm to limit ontogenetic effects (Elderfield et al., 2002). The tests were cleaned with distilled water using an ultrasonic bath to remove any contamination by external particles. The isotopic measurements were performed on a ThermoFisher Scientific MAT253 gas Isotope Ratio Mass Spectrometer coupled to a Kiel IV automated carbonate device at the Research Center for Geochronology and Isotopic

Geochemistry (CPGeo) from the University of São Paulo. Isotopic data used the Vienna Pee-Dee-Belemnite (VPDB) reference standard. Here we report the standard deviation of the laboratory reference material used for normalisation (SHP2L; Crivellari et al., 2021), being 0.07‰ (n=20 standards) over the measurement period. The standard deviation of the VPDB $\delta^{18}O$ values of the measured samples did not exceed 0.1‰. As no replicated measurements were carried out, we confirmed the consistency of our $\delta^{18}O$ values and value offset between *G. ruber* and *G. inflata* with the expected values for our study site. We verify this by comparing our records with published Holocene (Chiessi et al., 2007) and last glacial and interglacial stage (Santos et al., 2017b) datasets.

In addition, we use the abundances of the *Globorotalia truncatulinoides* right coiling form, as it has been documented to represent a well-mixed upper water column (reduced stratification), since this morphotype migrates to relatively shallower depths to complete its reproductive cycle (e.g., Lohmann and Schweitzer, 1990; Renaud and Schmidt, 2003; Feldmeijer et al., 2015; Billups et al., 2016).

3.6 Dissolution proxies

We quantify the effect of dissolution on foraminiferal assemblages by using: i) the ratio between the benthic and planktonic foraminifera (B/P ratio, Arrhenius, 1952; Parker and Berger, 1971; Kučera, 2007), ii) the number of whole planktonic foraminifera tests per gram of dry sediment (PF/g, Le and Shackleton, 1992; Suárez-Ibarra et al., 2021), iii) the abundance (%) of the coarse fraction i.e. larger than 63 μm (Berger et al., 1982; Gonzales et al., 2017; Suárez-Ibarra et al., 2021) and, iv) the $CaCO_3$ content (%) (Berger et al., 1982; Gonzales et al., 2017; Suárez-Ibarra et al., 2021). The $CaCO_3$ (%) was previously calculated by Rodrigues et al. (2018). The fraction >63 μm was estimated using a laser diffraction particle size analyzer Horiba Partica-LA-950X, which determined the grain size of the bulk sediment samples at the *Centro de Estudo de Geologia Costeira e Oceânica* (CECO) of the *Universidade Federal do Rio Grande do Sul* (UFRGS).

3.7 Multivariate statistical analyses

To divide the time series record into distinct cluster intervals (periods characterised by similar conditions) we carry out a clustering analysis. Posteriorly, to distinguish the dependencies of the grouping process we utilize an ordinate analysis. Both clustering and ordinate analyses are applied on the planktonic foraminifera species with relative abundances >1% (See Supplementary material).

Additionally, since all proxies are inevitably affected by different environmental processes other than the targeted parameters, we decrease the bias by also synthesising the variation through time of i) sea surface productivity, ii) upper water column stratification, and iii) carbonate dissolution. To do so, we run principal component analyses (PCA) on the above proxies, based on the correlation matrix. The data were centralised and standardised by dividing the difference between the dataset mean and the sample value by the dataset standard deviation. The synthesised productivity, stratification and dissolution proxies were extracted from the first axes of the PCAs as $PC1_P$ (productivity), $PC1_S$ (stratification) and $PC1_D$ (dissolution). Correlations between (and within) the first axes of the PCAs and other proxies were calculated using reduced major axis regressions. All PCA and correlation analyses were conducted using the software PAST (version 4.08; Hammer et al., 2001).

3.8 Spectral analysis

To test whether variations through time correspond to cyclic events, paced by orbital forcings, first we run a Multi-Taper-Method (MTM) test using the software "Acycle" (Li et al., 2019). The $PC1_P$ curve was detrended using a locally weighted scatterplot smoothing (LOWESS) and then analysed with the MTM. We set the smoother with a Time-bandwidth product of "2", and calculated the red noise following the Classical autoregressive (AR) model AR(1) (Husson, 2014). Second, we conducted a REDFIT spectral analysis utilising the software PAST (version 4.08; Hammer et al., 2001; Schulz and Mudelsee, 2002). The spectral analysis used the "Welch" window, a configuration of "4" for the oversampling and "2" as number of segments.

4 Results

The *G.bull*/*G.rub* ratio (Figure 2A) varies from 0.18 to 0.52 (mean 0.37 ± 0.09), increasing through MIS 5 up to the boundary with MIS 4 (90.1 to 75 ka) and again during MIS 3 (38.7 to 29.5 ka). Relative abundances of *G. glutinata* (Figure 2B) range between 4.9 and 24.8% (average 15 ± 4.05%) and show an increasing trend towards the MIS 5/4 boundary (from 91.9 to 72.7 ka). The BFAR (Figure 2C) varies between 11 (at 90 ka) and 230 $ind.cm^{-2}.kyr^{-1}$ (at 59 ka), with three intervals: first, a low decreasing trend from 105 to 87 ka (mean 27 $ind.cm^{-2}.kyr^{-1}$), followed by an abrupt jump and another decreasing trend from 84 to 39 ka (mean 92 $ind.cm^{-2}.kyr^{-1}$), and a final increasing trend until 30 ka (mean 67 $ind.cm^{-2}.kyr^{-1}$).

The abundance of *G. truncatulinoides* right coiling (Figure 2D) is low throughout the core (0 to 6.5%, mean 1.73). However, the 73–51 ka interval (approximately MIS 4) is marked by increased abundances and two abrupt peaks. The $\delta^{18}O_{G.rub}$ values range between -0.96 and 0.29‰ (mean -0.25 ± 0.33‰), with lower values during MIS 5, increasing towards MIS 4 and decreasing at the MIS 3 onset (Figure S1). The $\delta^{18}O_{G.inf}$ values vary between 0.56 and 1.56‰ (mean 1.16 ± 0.18‰) and display a progressively increasing trend from MIS 5 to MIS 3 (Figure S1). The $\delta^{18}O_{G.inf}$ record from core SIS-249 shows a good fit with the values from core GL-1090, except at 80 ka. The $\Delta\delta^{18}O$ between *G. inflata* and *G. ruber* (Figure 2E) presents values from 0.90 to 1.90‰ (mean 1.38 ± 0.24‰). $\Delta\delta^{18}O_{G.inf\text{-}G.rub}$ values are higher during MIS 5 (around 1.6‰), intermediate during MIS 3 (above 1.30‰), and generally lower during MIS 4 (mean 1.16 ± 0.18‰).

The B/P ratio (Figure 2F) ranges between 0.02 and 0.19, with low values during MIS 5d-c, an increase through MIS 5b, a reduction during MIS 5a (with a steep peak at 65 ka), followed by an increase at

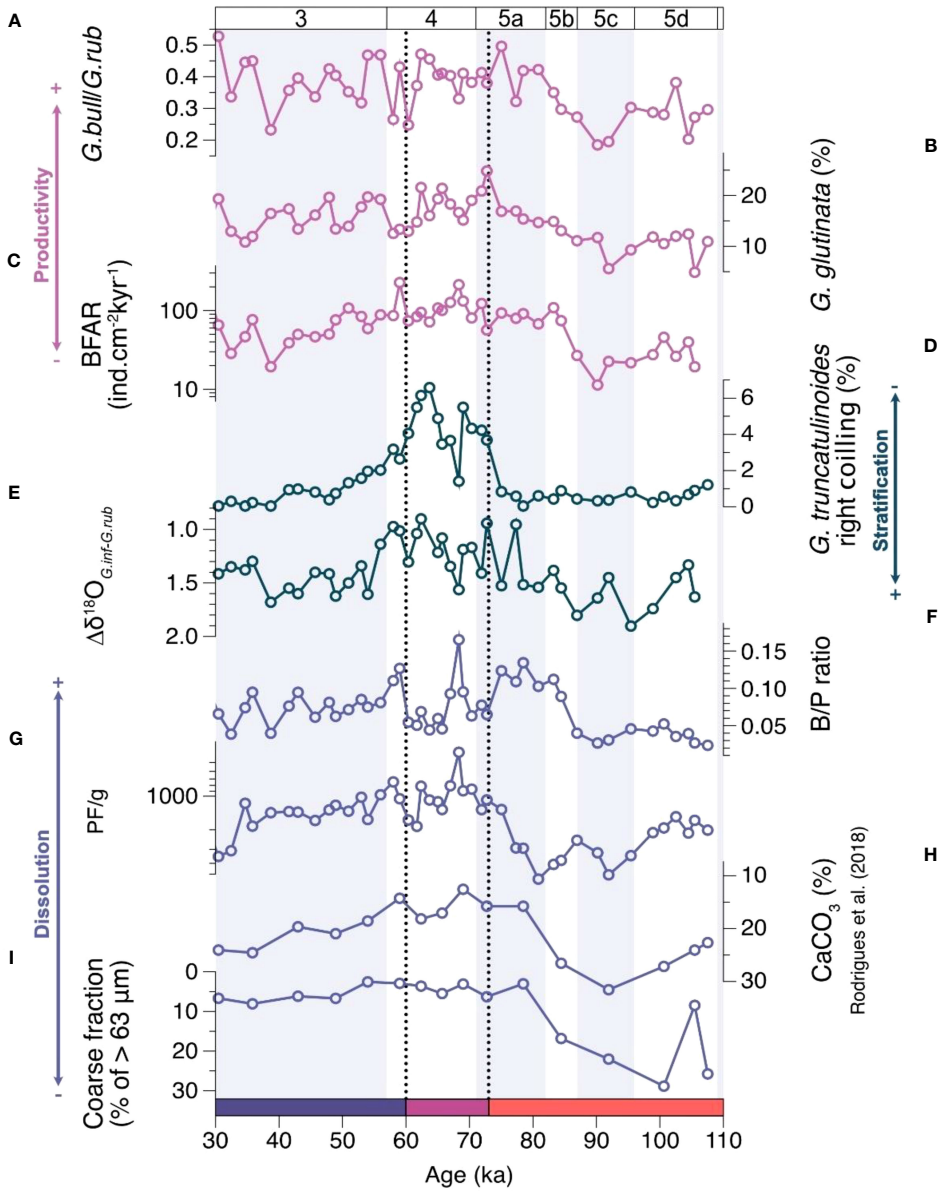

FIGURE 2
Time series records used to estimate productivity (in lilac: **(A)** *G. bulloides*/*G. ruber*, **(B)** *G. glutinata* abundance and **(C)** BFAR), stratification (in teal: **(D)** abundance of *G. truncatulinoides* right coiling and I $\Delta\delta^{18}O_{G.inf\text{-}G.rub}$), and dissolution (in steel blue: **(F)** B/P ratio, **(G)** PF/g, **(H)** $CaCO_3$ content (Rodrigues et al., 2018) and **(I)** >63 µm fraction). The black vertical dotted lines divide the record into biotic clusters where: Cluster I (red) is dominated by species characteristic of warm and oligotrophic water; cluster II (purple) by species related to eutrophic water, characterised by high productivity and low stratification; and cluster III (blue) by species from cooler waters. Y axes in **(E–I)** are reversed.

the end of MIS 4 and a further decrease with relatively stable values during MIS 3. The PF/g (Figure 2G) varies between 400 and 5540 (mean 1922 ± 1141 ind./g) and presents a decreasing trend from 91.9 to 70.3 ka, remaining low throughout MIS 4 and 3. The fraction coarser than 63 µm (Figure 2I) presents relatively high values (around 22%) during the 107–84 ka time interval, except at 105 ka when values drop to 8.5%. At 78 ka, values reach 3% and remain under 8% until the top of the record (30.4 ka). All the productivity, stratification, and dissolution proxies are shown in Figure 2.

Concerning the multivariate analyses, the first principal components of the PCA's analyses run on the productivity, stratification, and dissolution proxies ($PC1_P$, $PC1_S$ and $PC1_D$) synthesise 61.9, 78.6 and 66.4% of the variance, respectively. The results for the reduced major axis regressions within the $PC1_P$, $PC1_S$, $PC1_D$, $\delta^{13}C_{Uvig}$, accumulation rate (Acc. rates) and accumulation rates of total organic carbon (ARTOC) are shown in Table 1. All regression analyses show a significant (p <0.05) correlation except between $\delta^{13}C_{Uvig}$ and $PC1_D$.

Finally, the MTM spectral analyses yield significant results for the $PC1_P$ (supplementary material). The Classic AR(1) indicates the strongest power at the frequency 0.023 (>99%), associated with a 43 kyr-cycle (period = 1/frequency). The REDFIT points the strongest power also at the frequency 0.023 (>99%), associated with the same 43 kyr-cycle.

TABLE 1 Reduced major axis regression results.

RMA Regression	$PC1_P$-$PC1_S$	$PC1_P$- $\delta^{13}C_{Uvig}$	$PC1_P$-$PC1_D$	$\delta^{13}C_{Uvig}$-$PC1_D$	$PC1_P$-Acc. rates	$PC1_S$-Acc. rates	$PC1_S$-ARTOC
r:	**0.51**	**-0.32**	**0.80**	-0.28	**0.58**	**0.77**	**0.66**
r^2:	0.26	0.01	0.64	0.08	0.34	0.59	0.44
t:	3.90	-2.13	4.99	-1.07	4.62	7.79	3.20
p:	**<0.05**	**0.04**	**<0.05**	0.30	**<0.05**	**<0.05**	**0.01**
Permutation *p*:	**<0.05**	**0.04**	**<0.05**	0.31	**<0.05**	**<0.05**	**0.01**

In bold are significant (p <0.05) values. PC1 stands for first component axes of productivity ($PC1_P$) stratification ($PC1_S$), and dissolution ($PC1_D$) proxies. Accumulation rates (Acc. rates) were calculated according to the age model presented in this study. the accumulation rates of total organic carbon (TOC*AR) used data from Rodrigues et al. (2018).

5 Discussion

5.1 Upper water column conditions

The relatively high *G.bull*/*G.rub* ratios, *G. glutinata* (%) and BFAR values (Figures 2A–C) imply a period of enhanced sea surface productivity during MIS 4 and, to a lesser extent, MIS 3. The high glacial productivity recorded by core SIS-249 agrees with previous studies for the southern Brazilian continental margin (SBCM), that also document enhanced productivity during the last glacial stage (e.g., Gu et al., 2017; Pereira et al., 2018; Portilho-Ramos et al., 2019; Frozza et al., 2020; Suárez-Ibarra et al., 2022). The increase of around 40% in *G.bull*/*G.rub* mean ratios from ~0.27 (110–83 ka) to ~0.39 (83–30 ka) suggests an increase in the upwelling of subsurface more nutrient-rich South Atlantic Central Water (Venancio et al., 2016; Lessa et al., 2017; Lessa et al., 2019; Portilho-Ramos et al., 2019).

As the upwelling of subsurface waters necessarily implies a break in the upper water column stratification, we should also expect a similar behaviour in the stratification proxies. This can be primarily confirmed by the high relative abundances of *G. truncatulinoides* right coiling form, which also point to a less stratified, well-mixed upper water column during MIS 4 (Figure 2D, Lohmann and Schweitzer, 1990; Renaud and Schmidt, 2003; Feldmeijer et al., 2015; Billups et al., 2016; Pinho et al., 2021). Furthermore, *G. truncatulinoides* types II and V (right coiling forms) have also been associated with a shallow thermocline and eutrophic conditions (de Vargas et al., 2001; Ujiié and Lipps, 2009; Ujiié et al., 2010; Quillévéré et al., 2013). Finally, the less stratified upper water column during MIS 4 (and to a lesser extent MIS 3) is also supported by the lower $\Delta\delta^{18}O_{G.inf\text{-}G.rub}$values (Figure 2E), which implies a reduced stratification between the mixed layer and the thermocline (Santos et al., 2017b).

Considering that the utilised foraminiferal proxies also depend on other environmental parameters (for instance, changes in the relative abundances of one species can be due to variations in the abundances of other species), the use of the principal component analysis helps to synthesise the variation of the proxies through time. The $PC1_P$ (the synthesised first principal component of the *G.bull*/*G.rub* ratios, *G. glutinata* (%), and BFAR proxies) from our core SIS-249 (in the SBCM) suggests a transition, from MIS 5 to MIS 4, to more eutrophic conditions in the upper water column (Figure 3B). This shift in nutrient availability is also evident in the clustering and PCoA analyses (Figures S3 and S4), where the dominant/significant species shift from warm and oligotrophic conditions during MIS 5 (*G. ruber albus*, *O. universa* and *G. menardii*) to species associated with high productivity during MIS 4 (*G. glutinata, G. bulloides* and *G. truncatulinoides* dextral coiling). However, studies for the southeastern Brazilian continental margin (SEBCM) document a shift to less eutrophic conditions during the same time interval (e.g., Portilho-Ramos et al., 2015; Lessa et al., 2017; Lessa et al., 2019), associated with the eccentricity cycle. Our study suggests two different mechanisms fertilising the SBCM and SEBCM regions i) enhanced Fe-fertilisation through dust delivery and riverine input due to the strengthening of southwesterly winds during glacial stadials and ii) boosted upwelling delivering subsurface nutrient rich waters to the surface during interstadials, respectively.

Notably, our $PC1_P$ (along with the $PC1_S$ and $PC1_D$) varies alongside the obliquity cycle, as shown by the spectral analyses (Figure 3). The Classic AR(1) (Figure S5) and REDFIT (Figure S6) give a >99% confidence for our $PC1_P$ to be orbitally paced by the obliquity cycle (43 kyr). Our results support the hypothesis that the obliquity cycle modulates a dust delivered Fe-fertilising mechanism at the studied site (Lopes et al., 2021). Briefly, under low-obliquity values, annual average insolation decreases at the poles (Paillard, 2021), which would favour the expansion of Antarctica's ice sheets (Doughty et al., 2021), intensifying the southwesterly winds (SWW, Toggweiler et al., 2006) and the wind-driven dust delivery. Then, during low-obliquity intervals, the north limit of the SWW belt migrates north (from 40°S to 30°S latitude, Lamy et al., 2015; Gili et al., 2017) close to our coring site. This would allow the northward/offshore transport of more nutrient-rich, fresher, and cooler waters of the RdlP closer to our study area, also fertilising the photic zone (e.g., Gu et al., 2017; Pereira et al., 2018; Portilho-Ramos et al., 2019; Bottezini et al., 2021; Bottezini et al., 2022).

In fact, a northern/offshore influence of RdlP outflows during periods of low obliquity values would be supported by the population collapses of the dinoflagellate species *Operculodinium centrocarpum*, associated with the Brazil Current, documented by Gu et al. (2017) (core GeoB2107-3) for the SBCM during MIS 4 and the MIS 3/2 boundary (Figure 3D). Also, the decreased influence of the core of the Brazil Current (which transports warm oligotrophic water) in the study area would lead to a decrease in upper water column stratification, evidenced by our $PC1_S$ (Figure 3B). In addition, a northern/offshore intrusion of the nutrient-rich RdlP

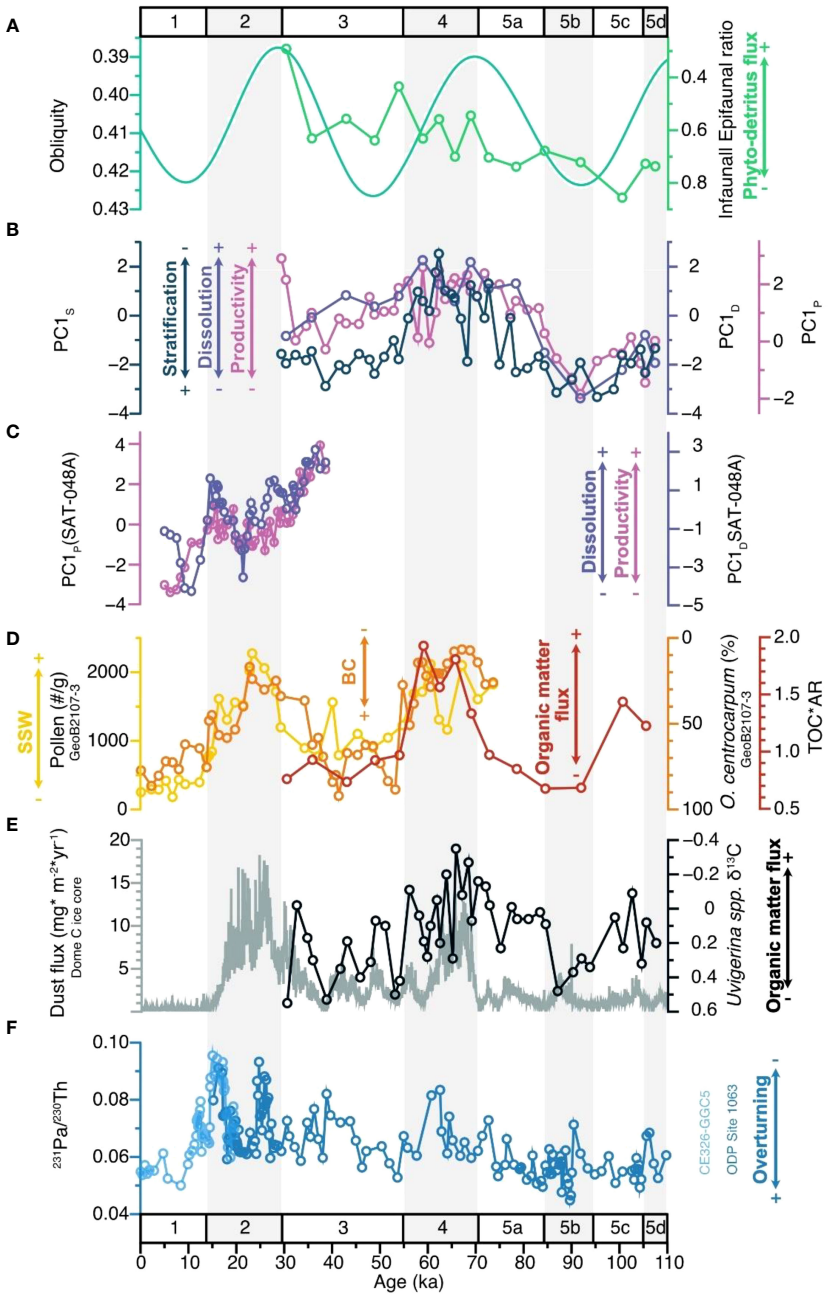

FIGURE 3
Time series graph showing the close relation between **(A)** obliquity values (Laskar et al., 2004), Infaunal/Epifaunal benthic foraminifera ratio by Rodrigues et al. (2018), and **(B)** the proxies for productivity ($PC1_P$), stratification ($PC1_S$) and dissolution ($PC1_D$) from core SIS-249. On **(C)**, synthesised record of productivity ($PC1_P$) and dissolution ($PC1_D$) from core SAT-048A (Suárez-Ibarra et al., 2022) and **(D)** SWW strength, as inferred by terrestrial pollen and the dinoflagellate species *O. centrocarpum* recorded by Gu et al. (2017, core GeoB2107-3, southern Brazilian continental margin), and the Total Organic Carbon (values from Rodrigues et al., 2018, also in core SIS-249) times the Accumulation Rates are shown. On **(E)**, the dust flux in Antarctica (Dome C ice core, Lambert et al., 2008) and core SIS-249 $\delta^{13}C_{Uvig}$ values (Rodrigues et al., 2018). Finally, on **(F)** the $^{231}Pa/^{230}Th$ proxy by McManus et al. (2004, light blue line, sediment core CE326-GGC5, 33°42'N, 57°35'W, 4550 mbsl) and Böhm et al. (2015, dark blue line, sediment core ODP Site 1063, Leg 172, 33°41'N, 57°37'W, 4,584 mbsl). Y axes in **(A)**, *O. centrocarpum* (%) and *Uvigerina* spp. $\delta^{13}C$ are reversed.

outflows (or freshwater bodies formed along the continental shelf) can also be inferred from the presence of freshwater diatoms during MIS 3–2 from core SIS-188 (Bottezini et al., 2021; Bottezini et al., 2022).

Moreover, strengthened SWW would also transport wind-driven particles from southern South America to the study area, increasing the Fe-fertilisation from terrestrial sources (Lopes et al., 2021). During MIS 5/4 and 3/2 boundaries, the elevated pollen concentrations (e.g., Gu et al., 2017, SBCM, core GeoB2107-3) can be interpreted as enhanced aeolian transport (Figure 3), and thus, terrestrial dust fertilisation. Additionally, the presence of the Andean pollen *Nothofagus*, recorded by Gu et al. (2017) during the late MIS 3 and MIS 2, corroborates the idea of enhanced windiness, strengthened SWW and aeolian Fe-fertilisation from

South American sources. On top of it, Lopes et al. (2021) compiled chemical studies analysing the provenance of glacial terrigenous dust in the southwest Atlantic, pointing southern South America (central-western Argentina and Patagonia) as the main source (e.g., Delmonte et al., 2010; Weber et al., 2012; Gili et al., 2017).

In summary, our record suggests two mechanisms to have fertilised the study area: i) upwelling, enhanced by the interplay of lower glacial sea level and the local bathymetry allowing the shoaling of nutrient-rich South Atlantic Central Water (also richer in silicic acid, Portilho-Ramos et al., 2019) to the sub-surface (e.g., Mahiques et al., 2007; Lessa et al., 2016) and; ii) obliquity-paced fertilisation from southern South America (wind-driven dust and the RdlP outflows) through enhanced aeolian transport, associated with expanded SWW. Both processes lead to a decrease in the upper water column stratification, first, by the ascension of cooler and less salty subsurface South Atlantic Central Water and, second, by the offshore displacement of the core of the Brazil Current. Ultimately, the correlation value between $PC1_P$ and $PC1_S$ (ρ<0.05, r=0.51) corroborates the synergy between the boosted biological pump and less stratified conditions.

5.2 Organic matter export and seafloor dynamics

Enhanced primary productivity (i.e., *G.bull*/*G.rub* and *G. glutinata* %) and decreased upper water column stratification ($PC1_S$) are mirrored by high accumulation rates of total organic carbon during MIS 4 (TOC*AR, Figure 3, TOC data from Rodrigues et al., 2018, and accumulation rates from this study). In addition, the BFAR proxy, commonly employed to reconstruct past surface productivity by examining organic matter export to the seafloor (Herguera and Berger, 1991), demonstrates significant co-variation (ρ<0.05) with both *G.bull*/*G.rub* (r=0.5) and *G. glutinata* relative abundances (r=0.55). Although the BFAR proxy has been widely used to quantitatively estimate past productivity changes, this relationship is not always straightforward (e.g., Naidu and Malmgren, 1995; Den Dulk et al., 2000; Jorissen et al., 2007). This limitation arises from the lack of calibration across various productivity settings, among other factors (for an in-depth discussion, please refer to Jorissen et al., 2007). However, Dias et al. (2021) demonstrated that the BFAR can indicate variations in the Cabo Frio Upwelling System, located in the SEBCM, where higher BFAR values correspond to increased export of fresh marine organic carbon.

The above-mentioned coupling suggests efficient glacial carbon sequestration via biological pump in the study area. A schematic representation of coupled benthic-pelagic changes observed in mid-latitude southwest Atlantic during the 107–30 ka time interval is presented in Figure 4.

The here evidenced increase in the export of organic matter (OM) to the seafloor from MIS 5 to MIS 4 (and to a lesser extent in MIS 3) aligns with the findings of Rodrigues et al. (2018). They observe a decrease in the infaunal/epifaunal benthic foraminifera ratio in core SIS-249, indicating a shift in the bioavailability of OM from refractory to labile forms (Gooday, 1993; Smart et al., 1994; Gooday, 2003; Garcia-Chapori et al., 2014; de Almeida et al., 2022). This change has significant implications for calcium carbonate preservation. As highlighted in our study, during phytoplankton blooms in glacial periods, higher amounts of OM (more labile, more soluble, and more easily remineralised) are exported to the seafloor, resulting in increased CO_2 release, lower pH, and the dissolution of $CaCO_3$ (Figure 4). In addition, despite the relatively brief sinking time of planktonic foraminifera tests (Takahashi and Bé, 1984; Schiebel and Hemleben, 2017), they could experience minor dissolution during transit through the CO_3^{2-} under-saturated intermediate SCWs (Frenz et al., 2003). These findings shed light on the important role of sea surface productivity and water mass properties in influencing the dynamics of carbonate preservation during different climatic periods.

Despite the sparser sampling in $PC1_D$ compared to $PC1_P$ and $PC1_S$, our study found a strong correlation between $PC1_P$ and $PC1_D$ in core SIS-249 (ρ<0.05, r=0.80, Table 1). This correlation supports the idea that enhanced dissolution is triggered by glacial high productivity, as it is also documented during the last deglaciation (Suárez-Ibarra et al., 2022, Figure 3C), even in deeper cores under the presence of modern non-corrosive Northern Component water. While inferring changes in paleoproductivity based on compositional assemblages from partially dissolved samples can be imprecise, our study addresses this issue by complementing the data with geochemical and sedimentological analyses. These additional analyses, like the $\delta^{18}O$ signal from the species *G. inflata* and *G. ruber* (both dissolution resistant according to experimental studies from Petró et al., 2018), as well as the BFAR and the TOC*AR, are less biased by dissolution.

Due to the OM enrichment in ^{12}C from photosynthesis (O'Leary, 1988; Ravelo and Hillaire-Marcel, 2007), remineralisation at the seafloor is expected to drive negative excursions in the endobenthic foraminiferal $\delta^{13}C$ values, as seen in MIS 5c and 4 (Figure 3E). Nevertheless, although $\delta^{13}C_{Uvig}$ is significantly anti correlated with our $PC1_P$ (ρ<0.05), the correlation value is weak (r=-0.31) and is likely impacted by additional changes in the dissolved inorganic carbon $\delta^{13}C$ of pore waters and/or the local bottom water mass geometry (Ravelo and Hillaire-Marcel, 2007; Hesse et al., 2014). Lopes et al. (2021) suggested an increased influence of more corrosive SCW at the core site during MIS 4 and 3, based on an apparent phasing between the $\delta^{13}C_{Uvig}$ record from core SIS-249 and the dust flux record from Dome C ice core (Lambert et al., 2008), as the dust-fertilisation in the Southern Ocean would be recorded in the $\delta^{13}C$ of the bottom water masses (Figure 3E). Although we do not exclude the possible influence of a higher proportion of SCW on carbonate preservation, our data show a relationship between the changes in the organic carbon cycle (periods of enhanced sea surface productivity associated with higher exportation of labile OM) and the deep-sea carbonate system. This highlights the need for further investigations applying a conservative or quasi-conservative water mass circulation tracer to elucidate the water masses mixing proportions at our site during the last glacial inception.

Furthermore, a third process that could have impacted the calcium carbonate preservation is the intensity of the Atlantic Meridional Overturning Circulation (AMOC). In a scenario with

10.3389/fevo.2023.1238334

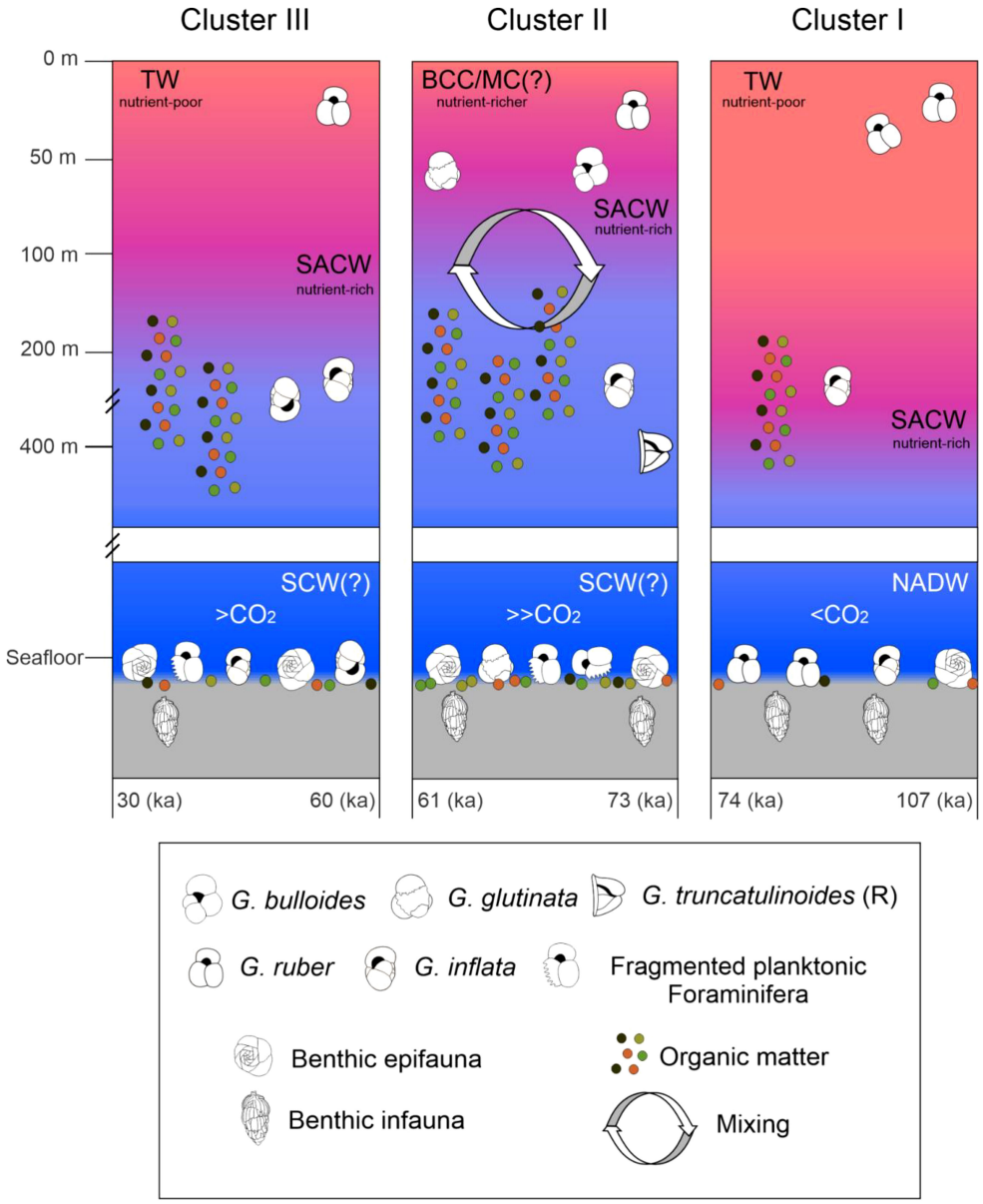

FIGURE 4
Schematic representation of main changes in sea surface and seafloor conditions recorded by core SIS-249 for the 107–30 ka interval, according to the foraminiferal assemblages and their respective three clusters. Interval I (107–74 ka) is dominated by species related to warm and oligotrophic water; species from interval II (73–61 ka) are related to eutrophic water, with high productivity and low stratification; and interval III (60–30 ka) is related to cooler water species. Interval II suggests higher levels of CO_2 at the seafloor mainly due to larger exports of OM. Benthic epifaunal and infaunal proportions, as well as TOC*AR.

a sluggish AMOC, the reduced water flow at the seafloor leads to an accumulation of respired CO_2, resulting in decreased water pH and subsequent corrosion of $CaCO_3$ (McManus et al., 2004; Thornalley et al., 2013; Howe et al., 2016b). Despite the lower temporal resolution of our $PC1_D$ record, it is evident that the positive excursions of $^{231}Pa/^{230}Th$ (Figure 3F), indicative of a sluggish AMOC (McManus et al., 2004; Böhm et al., 2015), do not align with the longer-term events of intense dissolution recorded by core SIS-249, which also seem to follow the 43 kyr-cycle. Furthermore, our findings are consistent with the conclusions of Suárez-Ibarra et al. (2022), who, using a dataset with higher temporal resolution, found that surface productivity was the primary factor driving calcium carbonate dissolution close to our study site.

Additionally, we would like to highlight that these processes, i) the biological pump and ii) water mass configuration, are not mutually exclusive and both may respond to the obliquity cycle. Under low obliquity values and decreased insolation at high latitudes, the (sub)polar fronts migrate equatorward: (i) displacing the north limit of the SSW belt closer to the study site, enhancing the wind-driven dust and continental river fertilisation, and boosting the biological pump; (ii) expanding the southern ice coverage, leading to an increased brine production and enhanced

SCW formation (Govin et al., 2009). This would result in the volumetric increase in the deep Atlantic of more corrosive SCWs which also act in part as a CO_2 storage reservoir.

Finally, although the enhanced remineralization causes part of the OM and biogenic carbonate to be recirculated back in the system instead of being exported to the sediments, we suggest an efficient biological pump in the mixed-layer, which removes inorganic carbon and points out the importance of the SBCM as a glacial carbon capture and sink of atmospheric CO_2 and thus part of the puzzle of glacial-interglacial CO_2 changes.

6 Conclusions

Based on our multiproxy analysis carried out in the sediments of core SIS-249, retrieved from the lower continental slope of the southwest Atlantic, southern Brazilian continental margin, we can conclude:

(i) In the study area, there was an increase in sea surface productivity from the last interglacial (MIS 5) to the subsequent glacial (MIS 4 and, partly, MIS 3). When compared to cores from the southeastern Brazilian continental margin, two possible fertilising mechanisms were identified: during glacial stadials the south was Fe-fertilised by enhanced dust delivery and riverine input due to the strengthening of southwesterly winds. During interstadials the southeastern region experienced expanded upwelling delivering subsurface nutrient rich waters to the surface.

(ii) Glacial increased continental aeolian-riverine fertilisation and reduced upper water column stratification led to an efficient removal of inorganic carbon via the biological pump, as evidenced by the high accumulation rates of total organic carbon, suggesting that the study area is capable to efficiently capture and sink atmospheric CO_2.

(iii) The degradation of the exported glacial organic matter can lead to decreased pH in bottom water, aiding dissolution and may play a major role in carbon sequestration irrespective of/addition to, deep water mass conditions.

Data availability statement

The datasets presented in this study can be found in online repositories. The names of the repository/repositories and accession number(s) can be found in the article/Supplementary Material.

Author contributions

Conceptualization – JS-I, TF, JC, MP; Data curation – JS-I, TF, CF; Formal Analysis – All; Funding acquisition – JS-I, JC, MP; Investigation – TF, MP; Methodology – JS-I, TF, CF, MP; Project administration – JC, MP; Resources – JS-I, JC, MP; Software – JS-I, CF, SC, MP; Supervision – TC, SC, TG-T, JC, MP; Validation – All; Visualization – JS-I, CF, SC, MP; Writing – original draft – JS-I, TF, CF; Writing – review & editing – All. All authors contributed to the article and approved the submitted version.

Funding

The author/s declare financial support was received for the research, authorship, and/or publication of this article. This work was funded by the Brazilian Coordination of Higher Education Staff Improvement–CAPES (grant number 88887.091729/2014-01), the Brazilian National Council for Scientific and Technological Development –CNPq (grant number 407922/2016-4) and the Charles University Grant Agency (GAUK, grant number 355422). JS-I thanks the STARS program (Přírodovědecká Fakulta, Univerzita Karlova), the ERASMUS+ program, the 4EU+ Alliance and the Johanna M. Resig Fellowship from the Cushman Foundation for Foraminiferal Research. TF thanks the CAPES and the DAAD for his MSc and PhD scholarships, respectively. CF thanks the CAPES for her PhD scholarship. TP acknowledges the AWI INSPIRES II program. BD appreciates financial support from FAPESP (grants 2022/01056-9, 2020/11452-3, and 2018/15123-4). MS thanks the STARS program (Přírodovědecká Fakulta, Univerzita Karlova). JC and MP acknowledge support from CNPq, grants 309394/2021-0 and 315684/2021-6, respectively.

Acknowledgments

The authors thank Rodrigo Portilho-Ramos, Thiago Santos, João Ballalai, Manuel F.G. Weinkauf and three reviewers for discussions through the development of this manuscript.

Conflict of interest

The authors declare that the research was conducted in the absence of any commercial or financial relationships that could be construed as a potential conflict of interest.

Publisher's note

Supplementary material

The Supplementary Material for this article can be found online at: https://www.frontiersin.org/articles/10.3389/fevo.2023.1238334/full#supplementary-material

References

Ahn, J., and Brook, E. J. (2008). Atmospheric CO2 and climate on millennial time scales during the last glacial period. *Science* 322, 83–85. doi: 10.1126/SCIENCE.1160832

Alves, E., Macario, K., Souza, R., Pimenta, A., Douka, K., Oliveira, F., et al. (2015). Radiocarbon reservoir corrections on the Brazilian coast from pre-bomb marine shells. *Quaternary Geochronology* 29, 30–35. doi: 10.1016/j.quageo.2015.05.006

Angulo, R. J., de Souza, M. C., Reimer, P. J., and Sasaoka, S. K. (2005). Reservoir effect of the southern and southeastern Brazilian coast. *Radiocarbon* 47, 67–73. doi: 10.1017/S0033822200052206

Archer, D., and Maier-Reimer, E. (1994). Effect of deep-sea sedimentary calcite preservation on atmospheric CO_2 concentration. *Nature* 367, 260–263. doi: 10.1038/367260a0

Arrhenius, G. (1952). Sediment cores from the east pacific. *Rep. Swedish Deep-Sea Expedition* 1947–1948 (5), 1–228.

Bé, A. W. H., and Hutson, W. H. (1977). Ecology of planktonic foraminifera and biogeographic patterns of life and fossil assemblages in the Indian ocean. *Micropaleontology* 23 (4), 369–414. doi: 10.2307/1485406

Berger, W. H., Bonneau, M.-C., and Parker, F. L. (1982). Foraminifera on the deep-sea floor: lysocline and dissolution rate. *Oceanologica Acta* 5 (2), 249–258.

Billups, K., Hudson, C., Kunz, H., and Rew, I. (2016). Exploring *Globorotalia truncatulinoides* coiling ratios as a proxy for subtropical gyre dynamics in the northwestern Atlantic Ocean during late Pleistocene Ice Ages. *Paleoceanography* 31, 553–563. doi: 10.1002/2016PA002927

Blaauw, M., and Christeny, J. A. (2011). Flexible paleoclimate age-depth models using an autoregressive gamma process. *Bayesian Anal.* 6, 457–474. doi: 10.1214/11-BA618

Böhm, E., Lippold, J., Gutjahr, M., Frank, M., Blaser, P., Antz, B., et al. (2015). Strong and deep atlantic meridional overturning circulation during the last glacial cycle. *Nature* 517, 73–76. doi: 10.1038/nature14059

Bottezini, S. R., Diniz, D., Ávila, A. S. P., and Leonhardt, A. (2022). Continental influence on the fertilization of marine waters during the Late Quaternary in the South of Brazilian Continental Margin. *Ocean Coast. Res.* 70, e22021. doi: 10.1590//2675-2824070.21072srb

Bottezini, S. R., Leonhardt, A., Diniz, D., and Ávila, A. S. P. (2021). Climatic and vegetational dynamics in Southern Brazil between 47.8 and 7.4 cal ka BP: a palynological analysis. *Rev. Bras. Paleontologia* 24, 345–356. doi: 10.4072/rbp.2024.4.05

Braga, E. S., Chiozzini, V. C., Berbel, G. B. B., Maluf, J. C. C., Aguiar, V. M. C., Charo, M., et al. (2008). Nutrient distributions over the Southwestern South Atlantic continental shelf from Mar del Plata (Argentina) to Itajaí (Brazil): Winter-summer aspects. *Continental Shelf Res.* 28, 1649–1661. doi: 10.1016/j.csr.2007.06.018

Broecker, W. S. (1982). Glacial to interglacial changes in ocean chemistry, Prog. *Oceanogr.* 11, 151–197. doi: 10.1016/0079-6611(82)90007-6

Broecker, W. S., and Peng, T. H. (1982). *Tracers in the Sea* (New York: Eldigio Press), 689.

Brovkin, V., Ganopolski, A., Archer, D., and Munhoven, G. (2012). Glacial CO_2 cycle as a succession of key physical and biogeochemical processes. *Clim. Past.* 8, 251–264. doi: 10.5194/cp-8-251-2012

Chalk, T. B., Foster, G. L., and Wilson, P. A. (2019). Dynamic storage of glacial CO_2 in the Atlantic Ocean revealed by boron $[CO_3^{2-}]$ and pH records. *Earth Planetary Sci. Lett.* 510, 1–11. doi: 10.1016/j.epsl.2018.12.022

Chiessi, C. M., Ulrich, S., Mulitza, S., Pätzold, J., and Wefer, G. (2007). Signature of the Brazil-Malvinas Confluence (Argentine Basin) in the isotopic composition of planktonic foraminifera from surface sediments. *Mar. Micropaleontology* 64, 52–66. doi: 10.1016/j.marmicro.2007.02.002

CLIMAP Project Members (1976). The surface of the ice-age earth. *Science* 191 (4232), 1131–1137. doi: 10.1126/science.191.4232.1131

Conan, S. M. H., and Brummer, G. J. A. (2000). Fluxes of planktic foraminifera in response to monsoonal upwelling on the Somalia Basin margin. *Deep Sea Res. Part II: Topical Stud. Oceanography* 47 (9-11), 2207–2227. doi: 10.1016/s0967-0645(00)00022-9

Conan, S. M. H., Ivanova, E. M., and Brummer, G. J. A. (2002). Quantifying carbonate dissolution and calibration of foraminiferal dissolution indices in the Somali Basin. *Mar. Geology* 182, 325–349. doi: 10.1016/S0025-3227(01)00238-9

Crivellari, S., Viana, P. J., de Carvalho Campos, M., Kuhnert, H., Lopes, A. B. M., da Cruz, F. W., et al. (2021). Development and characterization of a new in-house reference material for stable carbon and oxygen isotopes analyses. *J. Analytical Atomic Spectrometry* 36 (6), 1125–1134. doi: 10.1039/D1JA00030F

Curry, W. B., and Oppo, D. W. (2005). Glacial water mass geometry and the distribution of $\delta^{13}C$ of Sigma CO_2 in the western Atlantic Ocean. *Paleoceanography* 20, PA1017. doi: 10.1029/2004PA001021

de Almeida, K., Mello, R. M., Rodrigues, A. R., and Bastos, A. C. (2022). Bathymetric and regional benthic foraminiferal distribution on the Espírito Santo Basin slope, Brazil (SW Atlantic). *Deep Sea Res. Part I: Oceanographic Res. Papers* 181, 103688. doi: 10.1016/j.dsr.2022.103688

Delmonte, B., Andersson, P. S., Schöberg, H., Hansson, M., Petit, J. R., Delmas, R., et al. (2010). Geographic provenance of aeolian dust in East Antarctica during Pleistocene glaciations: preliminary results from Talos Dome and comparison with East Antarctic and new Andean ice core data. *Quaternary Sci. Rev.* 29 (1–2), 256–264. doi: 10.1016/j.quascirev.2009.05.010

Den Dulk, M., Reichart, G. J., van Heyst, S., Zachariasse, W. J., and van der Zwaan, G. J. (2000). Benthic foraminifera as proxies of organic matter flux and bottom water oxygenation? A case history from the northern Arabian Sea. *Palaeogeography Palaeoclimatology Palaeoecol.* 161, 337–359. doi: 10.1016/S0031-0182(00)00074-2

de Vargas, C., Renaud, S., Hilbrecht, H., and Pawlowski, J. (2001). Pleistocene adaptive radiation in *Globoratalia truncatulinoides*: genetic, morphologic, and environmental evidence. *Paleobiology* 27 (1), 104–125. doi: 10.1666/0094-8373(2001)027<0104:PARIGT>2.0.CO;2

Dias, B. B., Piotrowski, A. M., Barbosa, C. F., Venancio, I. M., Chiessi, C. M., and Albuquerque, A. L. S. (2021). Coupled changes in western south Atlantic carbón sequestration and particle reactive element cycling during millennial-scale Holocene climate variability. *Sci. Rep.* 11, 24378. doi: 10.1038/s41598-021-03821-8

Doss, W., and Marchitto, T. M. (2013). Glacial deep ocean sequestration of CO_2 driven by the eastern equatorial Pacific biologic pump. *Earth Planetary Sci. Lett.* 377-378, 45–54. doi: 10.1016/j.epsl.2013.07.019

Doughty, A. M., Kaplan, M. R., Peltier, C., and Barker, S. (2021). A maximum in global glacier extent during MIS 4. *Quaternary Sci. Rev.* 261, 106948. doi: 10.1016/j.quascirev.2021.106948

Duplessy, J. C., Shackleton, N. J., Fairbanks, R. G., Labeyrie, L., Oppo, D., and Kallel, N. (1988). Deepwater source variations during the last climatic cycle and their impact on the global deepwater circulation. *Paleoceanography* 3 (3), 343–360. doi: 10.1029/pa003i003p00343

Elderfield, H., Vautravers, M., and Cooper, M. (2002). The relationship between shell size and Mg/Ca, Sr/Ca, $\delta^{18}O$, and $\delta^{13}C$ of species of planktonic foraminifera. *Geochemistry Geophysics Geosystems* 3, 1–13. doi: 10.1029/2001GC000194

Emiliani, C. (1954). Depth habitats of some species of pelagic foraminifera as indicated by oxygen isotope ratios. *Am. J. Sci.* 252 (3), 149–158. doi: 10.2475/ajs.252.3.149

Feldmeijer, W., Metcalfe, B., Brummer, G.-J. A., and Ganssen, G. M. (2015). Reconstructing the depth of the permanent thermocline through the morphology and geochemistry of the deep dwelling planktonic foraminifer *Globorotalia truncatulinoides*. *Paleoceanography* 30, 1–22. doi: 10.1002/2014PA002687

Frenz, M., and Henrich, R. (2007). Carbonate dissolution revealed by silt grain-size distribution: Comparison of Holocene and Last Glacial Maximum Sediments from the Pelagic South Atlantic. *Sedimentology* 54, 391–404. doi: 10.1111/j.1365-3091.2006.00841.x

Frenz, M., Höppner, R., Stuut, J.-B. W., Wagner, T., and Henrich, R. (2003). "Surface sediment bulk geochemistry and grain-size composition related to the oceanic circulation along the south american continental margin in the southwest atlantic," in *The South Atlantic in the Late Quaternary*. Eds. G. Wefer, S. Mulitza and V. Ratmeyer. (Berlin, Heidelberg, New York, Tokyo: Springer-Verlag), 347–373. doi: 10.1007/978-3-642-18917-3_17

Frozza, C. F., Pivel, M. A. G., Suarez-Ibarra, J. Y., Ritter, M. N., and Coimbra, J. C. (2020). Bioerosion on late Quaternary planktonic Foraminifera related to paleoproductivity in the western South Atlantic. *Paleoceanography Paleoclimatology* 35, e2020PA003865. doi: 10.1029/2020pa003865

Garcia-Chapori, N., Laprida, C., Watanabe, S., Totah, V., and Violante, R. A. (2014). Mid-Late Pleistocene benthic foraminifera from Southwestern South Atlantic: driven by primary productivity or water mass properties? *Micropaleontology* 60, 195–210. doi: 10.47894/mpal.60.2.03

Gili, S., Gaiero, D. M., Goldstein, S. L., Chemale, F. Jr., Jweda, J., Kaplan, M. R., et al. (2017). Glacial/interglacial changes of Southern Hemisphere wind circulation from the geochemistry of South American dust. *Earth Planetary Sci. Lett.* 469, 98–109. doi: 10.1016/j.epsl.2017.04.007

Gonzales, M. V., de Almeida, F. K., Costa, K. B., Santarosa, A. C. A., Camillo, E., de Quadros, J. P., et al. (2017). Help INDEX: *Hoenglundina elegans* preservation index for marine sediments in the western South Atlantic. *J. Foraminiferal Res.* 47, 56–69. doi: 10.2113/gsjfr.47.1.56

Gooday, A. J. (1993). Deep-sea benthic foraminiferal species which exploit phytodetritus: characteristic features and controls on distribution. *Mar. Micropaleontology* 22 (3), 187–205. doi: 10.1016/0377-8398(93)90043-W

Gooday, A. J. (2003). Benthic foraminifera (Protista) as tools in deep-water palaeoceanography: environmental influences on faunal characteristics. *Adv. Mar. Biol.* 46, 1–90. doi: 10.1016/S0065-2881(03)46002-1

Gordon, A. L. (1989). Brazil-malvinas confluence-1984. *Deep Sea Res. Part A. Oceanographic Res. Papers* 36, 359–361. doi: 10.1016/0198-0149(89)90042-3

Gordon, A. L., and Greengrove, C. L. (1986). Geostrophic circulation of the Brazil-Falkland confluence. *Deep-Sea Res.* 33 (5), 573–585. doi: 10.1016/0198-0149(86)90054-3

Govin, A., Chiessi, C. M., Zabel, M., Sawakuchi, A. O., Heslop, D., Hörner, T., et al. (2014). Terrigenous input off northern South America driven by changes in Amazonian climate and the North Brazil Current retroflection during the last 250 ka. *Clim. Past* 10, 843–862. doi: 10.5194/cp-10-843-2014

Govin, A., Michel, E., Labeyrie, L., Waelbroeck, C., Dewilde, F., and Jansen, E. (2009). Evidence for northward expansion of Antarctic Bottom Water mass in the Southern Ocean during the last glacial inception. *Paleoceaonography* 24 (1), PA1202. doi: 10.1029/2008PA001603

Groeneveld, J., and Chiessi, C. M. (2011). Mg/Ca of *Globorotalia inflata* as a recorder of permanent thermocline temperatures in the South Atlantic. *Paleoceanography* 26, PA2203. doi: 10.1029/2010PA001940

Gu, F., Zonneveld, K. A., Chiessi, C. M., Arz, H. W., Pätzold, J., and Behling, H. (2017). Long-term vegetation, climate and ocean dynamics inferred from a 73,500 years old marine sediment core (GeoB2107-3) off southern Brazil. *Quaternary Sci. Rev.* 172, 55–71. doi: 10.1016/j.quascirev.2017.06.028

Guichard, S., Jorissen, F., Bertrand, P., Gervais, A., Martinez, P., Peypouquet, J. P., et al. (1997). Foraminifères benthiques et paléoproductivité: réflexions sur une carotte de l'*upwelling* (NW africain). *Comptes Rendus l'Académie Des. Sci. - Ser. IIA - Earth Planetary Sci.* 325, 65–70. doi: 10.1016/S1251-8050(97)83274-0

Hammer, Ø., Harper, D. A. T., and Ryan, P. D. (2001). PAST: Paleontological statistics software package for education and data analysis. *Palaeontologia Electronica* 4, 1–9.

Heaton, T. J., Köhler, P., Butzin, M., Bard, E., Reimer, R. W., Austin, W. E. N., et al. (2020). Marine20—The marine radiocarbon age calibration curve (0–55,000 cal BP). *Radiocarbon* 62, 779–820. doi: 10.1017/RDC.2020.68

Herguera, J. C., and Berger, W. H. (1991). Paleoproductivity from benthic foraminifera abundance: Glacial to postglacial change in the west equatorial Pacific. *Geology* 19 (12), 1173–1176. doi: 10.1130/0091-7613(1991)019%3C1173:PFBFAG%3E2.3.CO;2

Hesse, T., Wolf-Gladrow, D., Lohmann, G., Bijma, J., Mackensen, A., and Zeebe, R. E. (2014). Modeling $\delta^{13}C$ in benthic foraminifera: insights from model sensitivity experiments. *Mar. Micropaleontology* 112, 50–61. doi: 10.1016/j

Howe, J. N. W., Huang, K.-F., Oppo, D. W., Chiessi, C. M., Mulitza, S., Blusztajn, J., et al. (2018). Similar mid-depth atlantic water mass provenance during the last glacial maximum and heinrich stadial 1. *Earth Planetary Sci. Lett.* 490, 51–61. doi: 10.1016/j.epsl.2018.03.006

Howe, J. N. W., Piotrowski, A. M., Noble, T. L., Mulitza, S., Chiessi, C. M., and Baton, G. (2016a). North atlantic deep water production during the last glacial maximum. *Nat. Commun.* 7, 11765. doi: 10.1038/ncomms11765

Howe, J. N. W., Piotrowski, A. M., Oppo, D. W., Huang, K. F., Mulitza, S., Chiessi, C., et al. (2016b). Antarctic intermediate water circulation in the South Atlantic over the past 25,000 years. *Paleoceanography* 31, 1302–1314. doi: 10.1002/2016PA002975

Husson, D. (2014). *MathWorks File Exchange: RedNoise_ConfidenceLevels*. Available at: https://www.mathworks.com/matlabcentral/fileexchange/45539-rednoise_confidencelevels.

Jorissen, F. J., Fontanier, C., and Thomas, E. (2007). Paleoceanographical proxies based on deep-sea benthic foraminiferal assemblage characteristics. *Developments Mar. Geology* 1, 263–325. doi: 10.1016/S1572-5480(07)01011-1

Kučera, M. (2007). Planktonic foraminifera as tracers of past oceanic environments. *Developments Mar. Geology* 1, 213–262. doi: 10.1016/S1572-5480(07)01011-1

Lambert, F., Delmonte, B., Petit, J. R., Bigler, M., Kaufmann, P. R., Hutterli, M. A., et al. (2008). Dust-climate couplings over the past 800,000 years from the EPICA Dome C ice core. *Nature* 452, 616–619. doi: 10.1038/nature06763

Lamy, F., Arz, H.W., Kilian, R., Lange, C. B., Lembke-Jene, L., Wengler, M., et al. (2015). Glacial reduction and millennial-scale variations in Drake Passage through flow. *Proc. Natl. Acad. Sci.* 112, 13496–13501. doi: 10.1073/pnas.1509203112

Laskar, J., Robutel, P., Joutel, F., Gastineau, M., Correia, A. C. M., and Levrard, B. (2004). A long term numerical solution for the insolation quantities of the Earth. *A A* 428, 261–285. doi: 10.1051/0004-6361:20041335

Le, J., and Shackleton, N. J. (1992). Carbonate dissolution fluctuations in the western equatorial Pacific during the late Quaternary. *Paleoceanography* 7, 21–42. doi: 10.1029/91PA02854

Lessa, D., Morard, R., Jonkers, L., Venancio, I. M., Reuter, R., Baumeister, A., et al. (2020). Distribution of planktonic foraminifera in the subtropical South Atlantic: depth hierarchy of controlling factors. *Biogeosciences* 17, 4313–4342. doi: 10.5194/bg-17-4313-2020

Lessa, D. V. O., Ramos, R. P., Barbosa, C. F., da Silva, A. R., Belem, A., Turcq, B., et al. (2014). Planktonic foraminifera in the sediment of a western boundary upwelling system off Cabo Frio, Brazil. *Marine Micropaleontology*. *106* 55–68. doi: 10.1016/j.marmicro.2013.12.003

Lessa, D. V. O., Santos, T. P., Venancio, I. M., and Albuquerque, A. L. S. (2017). Offshore expansion of the Brazilian coastal upwelling zones during Marine Isotope Stage 5. *Global Planetary Change* 158, 13–20. doi: 10.1016/j.gloplacha.2017.09.006

Lessa, D. V. O., Santos, T. P., Venancio, I. M., Santarosa, A. C. A., dos Santos Junior, E. C., Toledo, F. A. L., et al. (2019). Eccentricity-induced expansions of Brazilian coastal upwelling zones. *Global Planetary Change* 179, 33–42. doi: 10.1016/j.gloplacha.2019.05.002

Lessa, D. V., Venancio, I. M., dos Santos, T. P., Belem, A. L., Turcq, B. J., Sifeddine, A., et al. (2016). Holocene oscillations of southwest atlantic shelf circulation based on planktonic foraminifera from an upwelling system (Off cabo frio, southeastern Brazil). *Holocene* 26 (8), 1175–1187. doi: 10.1177/0959683616638433

Li, M., Hinnov, L. A., and Kump, L. R. (2019). Acycle: Time-series analysis software for paleoclimate projects and education. *Comput. Geosciences* 127, 12–22. doi: 10.1016/j.cageo.2019.02.011

Lisiecki, L. E., and Raymo, M. E. (2005). A Pliocene–Pleistocene stack of 57 globally distributed benthic $\delta^{18}O$ records. *Paleoceanography* 20, PA1003. doi: 10.1029/2004PA001071

Locarnini, R. A., Mishonov, A. V., Antonov, J. I., Boyer, T. P., Garcia, H. E., Baranova, O. K., et al. (2013). "World ocean atlas 2013, volume 1: temperature,", vol. 73 . Eds. S. Levitus and A. Mishonov (NOAA Atlas NESDIS), (Maryland, USA: World ocean atlas 2013) 1, 40.

Lohmann, G. P., and Schweitzer, P. N. (1990). Globorotalia truncatulinoides' Growth and chemistry as probes of the past thermocline: 1. Shell size. *Paleoceanography* 5 (1), 55–755. doi: 10.1029/PA005i001p00055

Lopes, R. P., Bonetti, C., Dos Santos, G. S., Pivel, M. A. G., Petró, S. M., Caron, F., et al. (2021). Late Pleistocene sediment accumulation in the lower slope off the Rio Grande terrace, southern Brazilian Continental Margin. *Quaternary Int.* 571, 97–116. doi: 10.1016/j.quaint.2020.12.022

Mahiques, M. M., Fukumoto, M. M., Silveira, I. C. A., Figueira, R. C. L., Bícego, M. C., Lourenço, R. A., et al. (2007). Sedimentary changes on the southeastern Brazilian upper slope during the last 35,000 years. *Acad. Bras. Ciênc.* 79 (1), 171–181. doi: 10.1590/S0001-37652007000100018

Martin, J. H. (1990). Glacial-interglacial CO_2 change: the iron hypothesis. *Paleoceanography* 5 (1), 1–13. doi: 10.1029/PA005i001p00001

Matano, R. P., Combes, V., Piola, A. R., Guerrero, R., Palma, E. D., Strub, P. T., et al. (2014). The salinity signature of the cross-shelf exchanges in the Southwestern Atlantic Ocean: Numerical simulations. *J. Geophysical Research: Oceans* 119, 7949–7968. doi: 10.1002/2014JC010116

McManus, J. F., Francois, R., Gherardi, J.-M., Keigwin, L. D., and Brown-Leger, S. (2004). Collapse and rapid resumption of atlantic meridional circulation linked to deglacial climate changes. *Nature* 428 (6985), 834–837. doi: 10.1038/nature02494

Menking, J. A., Shackleton, S. A., Bauska, T. K., Buffen, A. M., Brook, E. J., Barker, S., et al. (2022). Multiple carbon cycle mechanisms associated with the glaciation of Marine Isotope Stage 4. *Nat. Commun.* 13, 5443. doi: 10.1038/s41467-022-33166-3

Mohtadi, M., Max, L., Hebbeln, D., Baumgart, A., Krück, N., and Jennerjahn, T. (2007). Modern environmental conditions recorded in surface sediment samples off W and SW Indonesia: Planktonic foraminifera and biogenic compounds analyses. *Mar. Micropaleontology* 65 (1–2), 96–112. doi: 10.1016/j.marmicro.2007.06.004

Möller, O. O., Piola, A. R., Freitas, A. C., and Campos, E. J. D. (2008). The effects of river discharge and seasonal winds on the shelf off southeastern South America. *Continental Shelf Res.* 28, 1607–1624. doi: 10.1016/j.csr.2008.03.012

Nadal De Masi, M. A. (1999). *Prehistoric hunter-gatherer mobility on the southern Brazilian coast: Santa Catarina Island* (Stanford University), 186. PhD dissertation.

Naidu, P. D., and Malmgren, B. A. (1995). Do benthic foraminifer records represent a productivity index in oxygen minimum zone areas? An evaluation from the Oman Margin, Arabian Sea. *Mar. Micropaleontology* 26, 49–55. doi: 10.1016/0377-8398(95)00014-3

O'Leary, M. H. (1988). Carbon Isotopes in Photosynthesis: Fractionation techniques may reveal new aspects of carbon dynamics in plants. *BioScience* 38 (5), 328–336. doi: 10.2307/1310735

Paillard, D. (2021). "Climate and astronomical cycles," in *Paleoclimatology*. Ed. G. Ramstein, et al (Switzerland: Springer Nature). doi: 10.1007/978-3-030-24982-3_28

Paillard, D., Labeyrie, L., and Yiou, P. (1996). Macintosh program performs time-series analysis. *Eos Trans. AGU* 77 (39), 379–379. doi: 10.1029/96EO00259

Parker, F. L., and Berger, W. H. (1971). Faunal and solution patterns of planktonic Foraminifera in surface sediments of the South Pacific. *Deep-Sea Res.* 18 (1), 73–107. doi: 10.1016/0011-7471(71)90017-9

Patterson, R. T., and Fishbein, A. (1989). Re-examination of the statistical methods used to determine the number of point counts needed for micropaleontological quantitative research. *Paleontological Soc.* 63, 245–248. doi: 10.1017/S0022336000019272

Peeters, F. J. C., Brummer, G. J. A., and Ganssen, G. (2002). The effect of upwelling on the distribution and stable isotope composition of *Globigerina bulloides* and *Globigerinoides ruber* (planktic foraminifera) in modern surface waters of the NW Arabian Sea. *Global Planetary Change* 34 (3–4), 269–291. doi: 10.1016/S0921-8181(02)00120-0

Peeters, F., Ivanova, E., Conan, S., Brummer, G.-J., Ganssen, G., Troelstra, S., et al. (1999). A size analysis of planktic Foraminifera from the Arabian Sea. *Mar. Micropaleontology* 36 (1), 31–61. doi: 10.1016/S0377-8398(98)00026-7

Pereira, L. S., Arz, H. W., Pätzold, J., and Portilho-Ramos, R. C. (2018). Productivity evolution in the South Brazilian Bight during the last 40,000 years. *Paleoceanography Paleoclimatology* 33, 1339–1356. doi: 10.1029/2018PA003406

Peterson, R. G., and Stramma, L. (1991). Upper-level circulation in the south atlantic ocean. *Prog. Oceanography* 26, 1–73. doi: 10.1016/0079-6611(91)90006-8

Petró, S. M., Pivel, M. A. G., and Coimbra, J. C. (2018). Foraminiferal solubility rankings: A contribution to the search for consensus. *J. Foraminiferal Res.* 48 (4), 301–313. doi: 10.2113/gsjfr.48.4.301

Petró, S. M., Pivel, M. A. G., and Coimbra, J. C. (2021). Evidence of supra-lysoclinal dissolution of pelagic calcium carbonate in the late Quaternary in the western South Atlantic. *Mar. Micropaleontology* 166, 102013. doi: 10.1016/j.marmicro.2021.102013

Pinho, T. M. L., Chiessi, C. M., Portilho-Ramos, R. C., Campos, M. C., Crivellari, S., Nascimento, R. A., et al. (2021). Meridional changes in the South Atlantic Subtropical Gyre during Heinrich Stadials. *Sci. Rep.* 11 (1), 9419. doi: 10.1038/s41598-021-88817-0

Piola, A. R., Campos, E. J., Möller, O. O. Jr., Charo, M., and Martinez, C. (2000). Subtropical shelf front off eastern South America. *J. Geophysical Research: Oceans* 105 (C3), 6565–6578. doi: 10.1029/1999JC000300

Piola, A. R., Matano, R. P., Palma, E. D., Möller, O. O. Jr., and Campos, E. J. (2005). The influence of the Plata River discharge on the western South Atlantic shelf. *Geophysical Res. Lett.* 32, L01603. doi: 10.1029/2004GL021638

Portilho-Ramos, R. C., Ferreira, F., Calado, L., Frontalini, F., and Toledo, M. B. (2015). Variability of the upwelling system in the southeastern Brazilian margin for the last 110,000 years. *Global Planetary Change* 135, 179–189. doi: 10.1016/j.gloplacha.2015.11.003

Portilho-Ramos, R. C., Pinho, T. M. L., Chiessi, C. M., and Barbosa, C. F. (2019). Understanding the mechanisms behind high glacial productivity in the southern Brazilian margin. *Climate Past* 15, 943–955. doi: 10.5194/cp-15-943-2019

Quillévéré, F., Morard, R., Escarguel, G., Douady, C. J., Ujiié, Y., de Garidel-Thoron, T., et al. (2013). Global scale same-specimen morpho-genetic analysis of *Truncorotalia truncatulinoides*: A perspective on the morphological species concept in planktonic foraminifera. *Palaeogeography Palaeoclimatology Palaeoecol.* 391, 2–12. doi: 10.1016/j.palaeo.2011.03.013

Ravelo, A. C., and Hillaire-Marcel, C. (2007). "The use of oxygen and carbon isotopes of foraminifera in paleoceanography," in *Proxies in Late Cenozoic Paleoceanography*. Eds. C. Hillaire-Marcel and A. Verna (Amsterdam: Developments in Marine Geology, Elsevier), 735–764.

Renaud, S., and Schmidt, D. N. (2003). Habitat tracking as a response of the planktic foraminifer *Globorotalia truncatulinoides* to environmental fluctuations during the last 140 kyr. *Mar. Micropaleontology* 49, 97–122. doi: 10.1016/S0377-8398(03)00031-8

Rickaby, R. E. M., Elderfield, H., Roberts, N., Hillenbrand, C.-D., and Mackensen, A. (2010). Evidence for elevated alkalinity in the glacial Southern Ocean. *Paleoceanography* 25 (1), PA1209. doi: 10.1029/2009PA001762

Rodrigues, A. R., Pivel, M. A. G., Schmitt, P., Almeida, F. K., and Bonetti, C. (2018). Infaunal and epifaunal benthic foraminifera species as proxies of organic matter paleofluxes in the Pelotas Basin, south-western Atlantic Ocean. *Mar. Micropaleontology* 144, 38–49. doi: 10.1016/j.marmicro.2018.05.007

Santos, T. P., Lessa, D. V. O., Venancio, I. M., Chiessi, C. M., Mulitza, S., Kuhnert, H., et al. (2017a). Stable oxygen isotope record during Termination II in sediment core GL1090. *PANGAEA*. doi: 10.1594/PANGAEA.884583

Santos, T. P., Lessa, D. O., Venancio, I. M., Chiessi, C. M., Mulitza, S., Kuhnert, H., et al. (2017b). The impact of the AMOC resumption in the western South Atlantic thermocline at the onset of the Last Interglacial. *Geophysical Res. Lett.* 44, 11–547. doi: 10.1002/2017GL074457

Sautter, L. R., and Thunell, R. C. (1991). Planktonic foraminiferal response to upwelling and seasonal hydrographic conditions; sediment trap results from San Pedro Basin, Southern California Bight. *J. Foraminiferal Res.* 21 (4), 347–363. doi: 10.2113/gsjfr.21.4.347

Schiebel, R., and Hemleben, C. (2017). *Planktic Foraminifers in the Modern Ocean*. (Berlin: Springer), 359.

Schlitzer, R. (2000). Electronic atlas of WOCE hydrographic and tracer data now available. *Eos Trans. Am. Geophysical Union* 81, 45–45. doi: 10.1029/00EO00028

Schlitzer, R. (2020). *Ocean Data View*. Available at: https://odv.awi.de.

Schulz, M., and Mudelsee, M. (2002). REDFIT: estimating red-noise spectra directly from unevenly spaced paleoclimatic time series. *Comput. Geosci.* 28 (3), 421–426. doi: 10.1016/S0098-3004(01)00044-9

Shackleton, S., Menking, J. A., Brook, E., Buizert, C., Dyonisius, M. N., Petrenko, V. V., et al. (2021). Evolution of mean ocean temperature in Marine Isotope Stage 4. *Climate Past* 17, 2273–2289. doi: 10.5194/cp-17-2273-2021

Sigman, D. M., and Boyle, E. A. (2000). Glacial/Interglacial variations in atmospheric carbon dioxide. *Nature* 407, 859–869. doi: 10.1038/35038000

Sigman, D. M., Hain, M. P., and Haug, G. H. (2010). The polar ocean and glacial cycles in atmospheric CO2 concentration. *Nature* 466, 47–55. doi: 10.1038/nature09149

Skinner, L. C. (2009). Glacial-interglacial atmospheric CO2 change: a possible "standing volume" effect on deep-ocean carbon sequestration. *Climate Past* 5, 537–550. doi: 10.5194/cp-5-537-2009

Smart, C. W., King, S. C., Gooday, A. J., Murray, J. W., and Thomas, E. (1994). A benthic foraminiferal proxy of pulsed organic matter paleofluxes. *Mar. Micropaleontology* 23 (2), 89–99. doi: 10.1016/0377-8398(94)90002-7

Souto, D. D., Lessa, D. V. O., Albuquerque, A. L. S., Sifeddine, A., Turcq, B. J., and Barbosa, C. F. (2011). Marine sediments from southeastern Brazilian continental shelf: A 1200 year record of upwelling productivity. *Palaeogeography Palaeoclimatology Palaeoecol.* 299, 49–55. doi: 10.1016/j.palaeo.2010.10.032

Stephens, B. B., and Keeling, R. F. (2000). The influence of Antarctic sea ice on glacial-interglacial CO_2 variations. *Nature* 404, 171–174. doi: 10.1038/35004556

Stramma, L., and England, M. (1999). On the water masses and mean circulation of the South Atlantic Ocean. *J. Geophysical Research: Oceans* 104 (C9), 20863–20883. doi: 10.1029/1999JC900139

Suárez-Ibarra, J. Y., Frozza, C. F., Palhano, P. L., Petró, S. M., Weinkauf, M. F. G., and Pivel, M. A. G. (2022). Calcium carbonate dissolution triggered by high productivity during the last glacial-interglacial interval in the deep western south atlantic. *Front. Earth Sci.* 10. doi: 10.3389/feart.2022.830984

Suárez-Ibarra, J. Y., Frozza, C. F., Petró, S. M., and Pivel, M. A. G. (2021). Fragment or broken? Improving the planktonic foraminifera fragmentation assessment. *PALAIOS* 36, 165–172. doi: 10.2110/palo.2020.062

Takahashi, K., and Bé, A. W. H. (1984). Planktonic Foraminifera: factors controlling sinking speeds. *Deep-Sea Res. Part Oceanogr Res. Pap.* 31, 1477–1500. doi: 10.1016/0198-0149(84)90083-9

Thornalley, D. J. R., Barker, S., Becker, J., Hall, I. R., and Knorr, G. (2013). Abrupt changes in deep Atlantic circulation during the transition to full glacial conditions. *Paleoceanography paleoclimatology* 28 (2), 253–262. doi: 10.1002/palo.20025

Toggweiler, J. R., Russell, J. L., and Carson, S. R. (2006). Midlatitude westerlies, atmospheric CO_2, and climate change during the ice ages. *Paleoceanography* 21, PA2005. doi: 10.1029/2005PA001154

Toledo, F., Costa, K. B., Pivel, M. A. G., and Campos, E. J. D. (2008). Tracing past circulation changes in the western South Atlantic based on planktonic Foraminifera. *Rev. Bras. Paleontologia* 11, 169–178. doi: 10.4072/rbp.2008.3.03

Ujiié, Y., de Garidel-Thoron, T., Watanabe, S., Wiebe, P., and de Vargas, C. (2010). Coiling dimorphism within a genetic type of the planktonic foraminifer *Globorotalia truncatulinoides*. *Mar. Micropaleontology* 77, 145–153. doi: 10.1016/j.marmicro.2010.09.001

Ujiié, Y., and Lipps, J. H. (2009). Cryptic diversity in planktic foraminifera in the Northwest Pacific Ocean. *J. Foraminiferal Res.* 39 (3), 145–154. doi: 10.2113/gsjfr.39.3.145

Venancio, I. M., Gomes, V. P., Belem, A. L., and Albuquerque, A. L. S. (2016). Surface-to-subsurface temperature variations during the last century in a western boundary upwelling system (Southeastern, Brazil). *Continental Shelf Res.* 125, 97–106. doi: 10.1016/j.csr.2016.07.003

Weber, M. E., Kuhn, G., Sprenk, D., Rolf, C., Ohlwein, C., and Ricken, W. (2012). Dust transport from Patagonia to Antarctica e A new stratigraphic approach from the Scotia Sea and its implications for the last glacial cycle. *Quat. Sci. Rev.* 36, 177–188. doi: 10.1016/j.quascirev.2012.01.016

Zaric, S., Donner, B., Fischer, G., Mulitza, S., and Wefer, G. (2005). Sensitivity of planktic foraminifera to sea surface temperature and export production as derived from sediment trap data. *Mar. Micropaleontology* 55 (1–2), 75–105. doi: 10.1016/j.marmicro.2005.01.002

Ziegler, M., Diz, P., Hall, I.R., and Zahn, R. (2013). Millennial-scale changes in atmospheric CO2 levels linked to the Southern Ocean carbon isotope gradient and dust flux. *Nat. Geosci.* 6, 457–461. doi: 10.1038/ngeo1782